

# A chip-scale, telecommunications-band frequency conversion interface for quantum emitters

Imad Agha,<sup>1,2,4,5</sup> Serkan Ates,<sup>1,2,4</sup> Marcelo Davanço,<sup>1,3</sup> and Kartik Srinivasan<sup>1,\*</sup>

<sup>1</sup>Center for Nanoscale Science and Technology, National Institute of Standards and Technology, Gaithersburg, MD 20899

<sup>2</sup>Maryland NanoCenter, University of Maryland, College Park, MD 20742

<sup>3</sup>Department of Applied Physics, California Institute of Technology, Pasadena, CA 91125

<sup>4</sup>These authors contributed equally.

<sup>5</sup>imad.agma@nist.gov

\*kartik.srinivasan@nist.gov

**Abstract:** We describe a chip-scale, telecommunications-band frequency conversion interface designed for low-noise operation at wavelengths desirable for common single photon emitters. Four-wave-mixing Bragg scattering in silicon nitride waveguides is used to demonstrate frequency upconversion and downconversion between the 980 nm and 1550 nm wavelength regions, with signal-to-background levels  $> 10$  and conversion efficiency of  $\approx -60$  dB at low continuous wave input pump powers ( $< 50$  mW). Finite element simulations and the split-step Fourier method indicate that increased input powers of  $\approx 10$  W (produced by amplified nanosecond pulses, for example) will result in a conversion efficiency  $> 25\%$  in existing geometries. Finally, we present waveguide designs that can be used to connect shorter wavelength (637 nm to 852 nm) quantum emitters with 1550 nm.

© 2018 Optical Society of America

**OCIS codes:** (350.4238) Nanophotonics and photonic crystals, (130.7405) Wavelength conversion devices, (270.0270) Quantum optics

## References and links

1. P. Michler, ed., *Single Semiconductor Quantum Dots* (Springer Verlag, Berlin, 2009).
2. C. Kurtsiefer, S. Mayer, P. Zarda, and H. Weinfurter, "Stable solid-state source of single photons," *Phys. Rev. Lett.* **85**, 290–293 (2000).
3. J. McKeever, A. Boca, A. D. Boozer, R. Miller, J. R. Buck, A. Kuzmich, and H. J. Kimble, "Deterministic generation of single photons from one atom trapped in a cavity," *Science* **303**, 1992–1994 (2004).
4. A. Beveratos, R. Brouri, T. Gacoin, A. Villing, J.-P. Poizat, and P. Grangier, "Single photon quantum cryptography," *Phys. Rev. Lett.* **89**, 187901 (2002).
5. E. Knill, R. Laflamme, and G. J. Milburn, "A scheme for efficient quantum computation with linear optics," *Nature* **409**, 46–52 (2001).
6. J. L. O'Brien, A. Furusawa, and J. Vučković, "Photonic quantum technologies," *Nature Photonics* **3**, 687–695 (2009).
7. C. Simon, M. Afzelius, J. Appel, A. Boyer de La Giroday, S. J. Dewhurst, N. Gisin, C. Y. Hu, F. Jelezko, S. Kröll, J. H. Müller, J. Nunn, E. S. Polzik, J. G. Rarity, H. de Riedmatten, W. Rosenfeld, A. J. Shields, N. Sköld, R. M. Stevenson, R. Thew, I. A. Walmsley, M. C. Weber, H. Weinfurter, J. Wrachtrup, and R. J. Young, "Quantum memories. A review based on the European integrated project "Qubit Applications (QAP)"", *European Physical Journal D* **58**, 1–22 (2010).
8. P. Kumar, "Quantum Frequency-Conversion," *Opt. Lett.* **15**, 1476–1478 (1990).

9. M. Raymer and K. Srinivasan, "Manipulating the color and shape of single photons," *Physics Today* **65**, 32–37 (2012).
10. M. T. Rakher, L. Ma, O. Slattery, X. Tang, and K. Srinivasan, "Quantum transduction of telecommunications-band single photons from a quantum dot by frequency upconversion," *Nature Photonics* **4**, 786–791 (2010).
11. S. Zaske, A. Lenhard, C. A. Keßler, J. Kettler, C. Hepp, C. Arend, R. Albrecht, W.-M. Schulz, M. Jetter, P. Michler, and C. Becher, "Visible-to-telecom quantum frequency conversion of light from a single quantum emitter," *Phys. Rev. Lett.* **109**, 147404 (2012).
12. S. Ates, I. Agha, A. Gulinatti, I. Rech, M. T. Rakher, A. Badolato, and K. Srinivasan, "Two-photon interference using background-free quantum frequency conversion of single photons emitted by an inas quantum dot," *Phys. Rev. Lett.* **109**, 147405 (2012).
13. K. de Greve, L. Yu, P. L. McMahon, J. S. Pelc, C. M. Natarajan, N. Y. Kim, E. Abe, S. Maier, C. Schneider, M. Kamp, S. Höfling, R. H. Hadfield, A. Forchel, M. M. Fejer, and Y. Yamamoto, "Quantum-dot spin-photon entanglement via frequency downconversion to telecom wavelength," *Nature* **491**, 421–425 (2012).
14. C. McKinstrie, J. Harvey, S. Radic, and M. Raymer, "Translation of quantum states by four-wave mixing in fibers," *Opt. Express* **13**, 9131–9142 (2005).
15. H. J. McGuinness, M. G. Raymer, C. J. McKinstrie, and S. Radic, "Quantum frequency translation of single-photon states in a photonic crystal fiber," *Phys. Rev. Lett.* **105**, 093604 (2010).
16. I. Agha, M. Davanço, B. Thurston, and K. Srinivasan, "Low-noise chip-based frequency conversion by four-wave-mixing bragg scattering in SiN<sub>x</sub> waveguides," *Opt. Lett.* **37**, 2997–2999 (2012).
17. K. Uesaka, K. Kin-Yip, M.E., Marhic, and L. Kazovsky, "Wavelength exchange in a highly nonlinear dispersion-shifted fiber: Theory and experiments," *IEEE J. Sel. Top. Quan. Elec.* **8**, 560–568 (2002).
18. K. Ikeda, R. E. Saperstein, N. Alic, and Y. Fainman, "Thermal and Kerr nonlinear properties of plasma-deposited silicon nitride/ silicon dioxide waveguides," *Opt. Express* **16**, 12987 (2008).
19. J. S. Levy, A. Gondarenko, M. A. Foster, A. C. Turner-Foster, A. L. Gaeta, and M. Lipson, "CMOS-compatible multiple-wavelength oscillator for on-chip optical interconnects," *Nature Photonics* **4**, 37–40 (2010).
20. D. T. H. Tan, K. Ikeda, P. C. Sun, and Y. Fainman, "Group velocity dispersion and self phase modulation in silicon nitride waveguides," *Appl. Phys. Lett.* **96**, 061101 (2010).
21. H. J. McGuinness, M. Raymer, C. McKinstrie, and S. Radic, "Wavelength translation across 210 nm in the visible using vector bragg scattering in a birefringent photonic crystal fiber," *IEEE Photonics Tech. Lett.* **23**, 109–111 (2011).
22. A. S. Clark, S. Shahnia, M. J. Collins, C. Xiong, and B. J. Eggleton, "High-efficiency frequency conversion in the single-photon regime," *Opt. Lett.* **38**, 947–949 (2013).
23. F. Ferdous, H. Miao, D. E. Leaird, K. Srinivasan, J. Wang, L. Chen, L. T. Varghese, and A. M. Weiner, "Spectral line-by-line pulse shaping of on-chip microresonator frequency combs," *Nature Photonics* **5**, 770–776 (2011).
24. M. A. Foster, J. S. Levy, O. Kuzucu, K. Saha, M. Lipson, and A. L. Gaeta, "Silicon-based monolithic optical frequency comb source," *Opt. Express* **19**, 14233–14239 (2011).
25. Y. Okawachi, K. Saha, J. S. Levy, Y. H. Wen, M. Lipson, and A. L. Gaeta, "Octave-spanning frequency comb generation in a silicon nitride chip," *Opt. Lett.* **36**, 3398–3400 (2011).
26. S. Ates, I. Agha, A. Gulinatti, I. Rech, A. Badolato, and K. Srinivasan, "Improving the performance of bright quantum dot single photon sources using temporal filtering via amplitude modulation," *Scientific Reports* **3**, 1397 (2013).
27. G. P. Agrawal, *Nonlinear Fiber Optics* (Academic Press, Amsterdam, 2007).
28. M. A. Foster, A. C. Turner, J. E. Sharping, B. S. Schmidt, M. Lipson, and A. L. Gaeta, "Broad-band optical parametric gain on a silicon photonic chip," *Nature* **441**, 960–963 (2006).
29. Q. Lin, O. J. Painter, and G. P. Agrawal, "Nonlinear optical phenomena in silicon waveguides: modeling and applications," *Opt. Express* **15**, 16604 (2007).
30. X. Liu, R. M. Osgood, Y. A. Vlasov, and W. M. J. Green, "Mid-infrared optical parametric amplifier using silicon nanophotonic waveguides," *Nature Photonics* **4**, 557–560 (2010).
31. S. Zlatanovic, J. S. Park, S. Moro, J. M. C. Boggio, I. B. Divliansky, N. Alic, S. Mookherjea, and S. Radic, "Mid-infrared wavelength conversion in silicon waveguides using ultracompact telecom-band-derived pump source," *Nature Photonics* **4**, 561–564 (2010).
32. K.-Y. Wang and A. C. Foster, "Ultralow power continuous-wave frequency conversion in hydrogenated amorphous silicon waveguides," *Opt. Lett.* **37**, 1331 (2012).

---

## 1. Introduction

Interfaces that connect photonic quantum systems operating at different frequencies constitute an important resource in the development of a hybrid architecture that leverages the key advantages of its component entities. Such hybrid architectures may be at the heart of modern quantum networks, which must be able to generate, send, manipulate, and store quantum infor-

mation with high fidelity and low loss. For example, single photon sources (SPSs) based on single quantum emitters like InAs quantum dots [1], nitrogen vacancy centers in diamond [2], and neutral alkali atoms [3] all exhibit desirable features, such as on-demand generation with the potential for high single photon purity and indistinguishability. These properties are crucial in both quantum cryptography [4] and quantum computing [5, 6] applications. Unfortunately, for these common quantum emitters, emission occurs at wavelengths below 1000 nm, where long-distance transmission through optical fibers is not optimal. Similarly, many promising quantum memories [7] operate in the visible or near-visible, whereas silicon-based systems that have been developed for applications in nanophotonics, CMOS electronics, and microelectromechanics are opaque at such wavelengths. Thus, interfaces that can connect disparate wavelength regions without otherwise disturbing the relevant properties of the quantum state (such as photon statistics and coherence time) are an important resource for future photonic quantum information processing systems. Such quantum frequency conversion [8, 9] has been demonstrated with single photon Fock states generated by single semiconductor quantum dots [10–13], where three-wave-mixing in periodically-poled lithium niobate waveguides was used for both upconversion [10, 12] and downconversion [11, 13].

Future applications may benefit from the development of such frequency conversion technology within silicon-based material systems, for which complex and highly scalable fabrication technology at a level beyond lithium niobate has been demonstrated. To that end, frequency conversion through four-wave-mixing Bragg scattering (FWM-BS) [14], a process used in quantum frequency conversion experiments in optical fibers [15], was recently demonstrated in silicon nitride ( $\text{Si}_3\text{N}_4$ ) waveguides [16], where  $\text{Si}_3\text{N}_4$  was chosen due to its wide optical transparency window (including visible and near-visible wavelengths of importance to many quantum optical systems), its relatively high nonlinear refractive index, and low linear and nonlinear absorption. In Ref. [16], narrowband conversion over a few nanometers was measured, and the low-noise nature was inferred by measuring the pump-induced noise. Here, we show the flexibility of FWM-BS in these  $\text{Si}_3\text{N}_4$  devices by demonstrating wideband downconversion and upconversion between the 980 nm and 1550 nm bands, with a signal-to-noise ratio  $\gtrsim 10$  as determined via photon counting measurements. Through calculations of waveguide dispersion and simulations using the split-step Fourier method, we further show that simple variations in the waveguide geometry should extend this technique to enable quantum emitters in the 637 nm, 780 nm, and 850 nm wavelength bands to be connected to the 1550 nm band. Finally, as the demonstrated conversion efficiencies are low ( $\approx -60$  dB) due to relatively low pump power used ( $< 50$  mW), we use simulations to establish the pump powers required to achieve conversion efficiencies high enough for realistic experiments with single photon states of light. We find that pump powers of  $\approx 10$  W, achievable through amplified nanosecond pulses, for example, should enable conversion efficiencies  $> 25$  % to be achieved.

## 2. Principle of operation

Four-wave-mixing Bragg scattering is a nonlinear mixing process involving four non-degenerate fields, whereby two pumps  $\omega_1$  and  $\omega_2$  mediate the scattering from a signal  $\omega_s$  to an idler  $\omega_i$ . In this paper, we consider a process in which the idler frequencies are given by  $\omega_i^\pm = \omega_2 \pm (\omega_s - \omega_1)$ . In the slowly-varying envelope approximation, and ignoring the effects of pump-depletion, the conversion efficiency from the signal to the idler at a propagation distance  $z$  along the waveguide is given by:

$$\eta(z) = \frac{4\gamma_1\gamma_2P_1P_2}{g^2} \sin^2(gz) \quad (1)$$

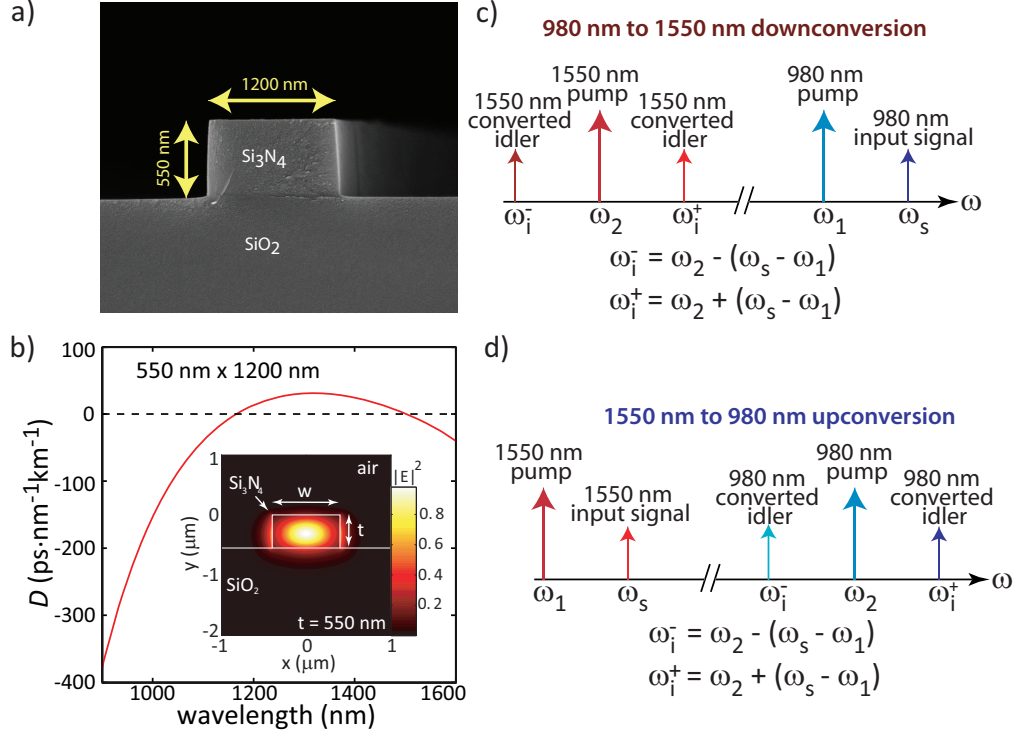


Fig. 1. a) Scanning electron microscope image of the 550 nm x 1200 nm silicon nitride waveguide used in the current experiment. b) Dispersion parameter  $D = \frac{-2\pi c}{\lambda^2} \frac{d^2\beta}{d\omega^2}$  as a function of wavelength  $\lambda$  ( $\beta$  is the propagation constant,  $c$  is the speed of light). The zero-dispersion point is around 1200 nm, as required by phase-matching considerations. The inset shows the numerically calculated electric field amplitude for the fundamental TE waveguide mode. c) and d) Position of the pumps, signal, and idlers in frequency space for frequency downconversion (c) and upconversion (d).

where  $\gamma_1$  and  $\gamma_2$  are the waveguide's effective nonlinearity parameter at the two pump wavelengths,  $P_1$  and  $P_2$  are the powers in pumps 1 and 2, respectively, and  $g$  is the four-wave-mixing gain that depends both on the pump powers (through nonlinear dispersion) and the linear phase mismatch [17]. A typical estimated value for the effective nonlinearity parameter is  $\gamma \approx 6 \text{ W}^{-1}\text{m}^{-1}$  (depending on the specific waveguide cross-section and wavelength), which is determined assuming a nonlinear refractive index  $n_2 = 2.5 \times 10^{-19} \text{ m}^2\text{W}^{-1}$  [18]. By tailoring the dispersion appropriately, and by having the two pumps widely separated in wavelength, this process allows ultra-wide band frequency conversion. Moreover, due to the fact that this is a wavelength exchange process with no net amplification of either signal or idler, the conversion is theoretically noiseless and is suitable for quantum state translation [14]. In reality, the noise limit may come either from poor filtering of the pumps or, in certain materials, from Raman scattering or other four-wave-mixing processes.

In this work, our main motivation is to develop an interface for frequency conversion from 980 nm to 1550 nm (InAs quantum dot SPSs to telecom wavelength) in a silicon nitride waveguide (Fig. 1(a)). Silicon nitride is chosen here due to CMOS fabrication compatibility [19], simple growth techniques, large transparency window, high optical nonlinearity (x10 that of

SiO<sub>2</sub>) [20], and low nonlinear loss (absence of two-photon absorption and free-carrier generation). Details on the fabrication technique and dispersion calculations (Fig. 1(b)) can be found in Ref. [16]. Unlike this earlier work, whereby we employed two telecom-band pumps to convert a signal to its idler in the 980 nm band, here we place one of pumps near 1550 nm and the other around 980 nm (Fig. 1(c,d)), allowing for downconversion (upconversion) over a  $\approx 600$  nm range, a significantly larger wavelength translation range compared to wideband conversion recently demonstrated in optical fibers through FWM-BS [21]. As the nonlinear phase-mismatch scales as  $\Delta\beta_{nl} = \gamma_1 P_1 - \gamma_2 P_2$ , where  $\gamma_1$  ( $\gamma_2$ ) is the nonlinear coefficient at  $\omega_1$  ( $\omega_2$ ) and  $\Delta\beta_{nl} \approx \gamma(P_1 - P_2)$  for two pumps in the same band [17], we use the same design parameters as [16] in our device fabrication. We produce 18 mm long, 550 nm x 1200 nm (height x width) Si<sub>3</sub>N<sub>4</sub>-on-SiO<sub>2</sub> waveguides with an air top cladding, and can adjust the ratio of pump powers to eliminate the nonlinear phase mismatch. In this experiment, a straight waveguide was employed, however, mature fabrication techniques (both in writing and etching the structure) and the index contrast between Si<sub>3</sub>N<sub>4</sub> and SiO<sub>2</sub> allow for integrating the same length in a much smaller ( $\approx 1$  mm) footprint via a spiral layout.

### 3. Experimental results - Wideband Frequency Downconversion

The experimental setup for frequency downconversion of a 980 nm band signal to a telecom-band idler is shown in Fig. 2(a). A strong (550 mW) pump consisting of a 974 nm distributed feedback laser is combined with a weak, tunable signal on a 90:10 coupler, and the combined output is sent to the 980 nm port of a 980 nm/1550 nm wavelength-division multiplexer (WDM). The signal power at the input of the waveguide is in the range of a few  $\mu$ W. The second pump is a 1550 nm laser that is amplified via an erbium-doped amplifier (EDFA) and sent to the other port of the WDM. The combined pumps and signal are coupled to the waveguide via a lensed fiber, and the output of the waveguide is filtered to reject both the residual (unconverted) signal and the pumps. This output is either sent to a spectrometer equipped with a cooled InGaAs photodiode array for spectral analysis, or is further bandpass-filtered and sent to an InGaAs single photon avalanche diode (SPAD) for signal-to-noise analysis. Data is synchronously recorded on the spectrometer while the 980 nm band signal laser is tuned from 965 nm to 985 nm in 0.2 nm steps and monitored on an optical spectrum analyzer (OSA).

Figure 2(b) shows the generated idlers in the 1550 nm band for a specific set of pump and input signal wavelengths in the 980 nm band (the 1550 nm pump has been removed by a notch filter after the WG chip, as shown in Fig. 2(a)). Tuning the signal away from the 974 nm pump causes the idlers to tune in accordance with energy conservation  $\omega_i = \omega_2 \pm (\omega_s - \omega_1)$ , as shown in the image plot in Fig. 2(c). Here, the x-axis is in units of detuning between the generated idlers and the fixed 1550 nm pump, while the y-axis is in units of detuning between the input 980 nm band signal and fixed 974 nm pump.

Figure 2(d) shows the normalized conversion efficiency as a function of the idler wavelength (for fixed pump wavelengths). This plot shows both the phase matching bandwidth of our device as well as oscillations which are likely due to its expected sinc<sup>2</sup> character (Eq. 1). We next use an InGaAs SPAD to determine both the conversion efficiency as well as the signal-to-background ratio for the converted idler as a function of the 1550 nm pump power. The signal-to-background is determined by measuring the counts in the  $\omega_i^+$  idler band with the input 980 nm signal on and off, and dividing the two values (after subtraction of the detector dark count rate of  $\approx 150$  s<sup>-1</sup>). As the pump power inside the waveguide and at its input is increased from 5 mW to 43 mW, the internal conversion efficiency (taking into account 7.5 dB input and output coupling losses) increases from -74 dB to -64 dB while the signal-to-background increases from  $\approx 5$  to  $\approx 10$ . While nearly background-free FWM-BS conversion has been demonstrated in situations for which the detuning between pumps and signal and idler is large [15], for

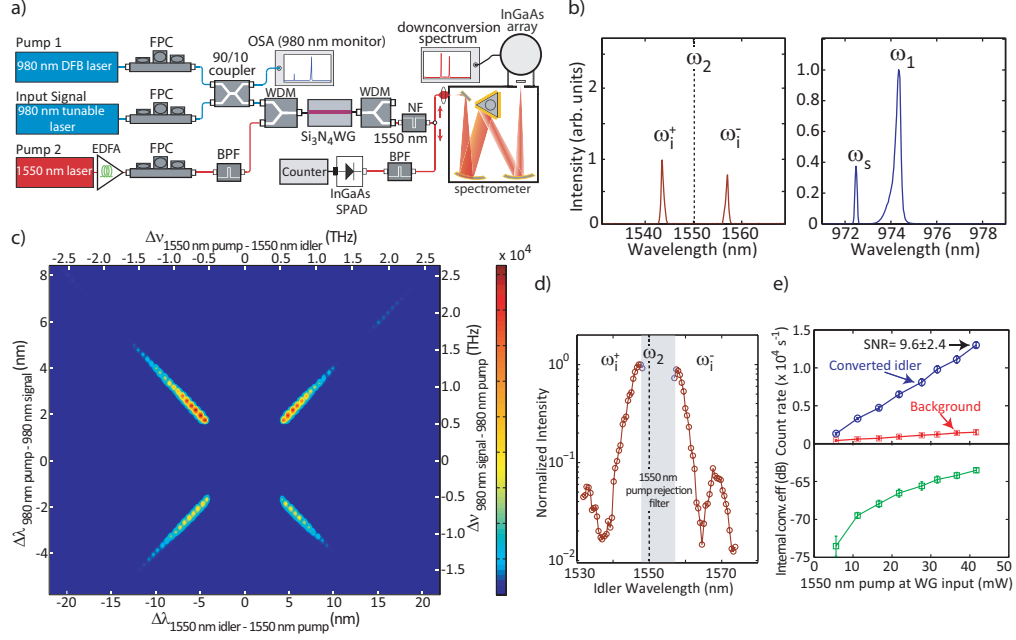


Fig. 2. a) Experimental setup for frequency downconversion from 980 nm to 1550 nm: A tunable 980 nm signal laser is combined with a strong 974 nm distributed feedback (DFB) pump laser and then multiplexed (through a fiber 980 nm/1550 nm wavelength-division multiplexer (WDM)) with a 1550 nm laser that is amplified via an erbium-doped fiber amplifier (EDFA). Fiber polarization controllers (FPCs) ensure that the signal and pumps are co-polarized and launched into the desired waveguide mode. An optical spectrum analyzer (OSA) monitors the 980 nm wavelengths, while the output of the waveguide is first filtered through a notch filter (NF) to remove the residual 1550 nm pump, and then either sent to an InGaAs spectrometer or through a bandpass filter (BPF) to an InGaAs single photon avalanche diode (SPAD). b) Sample spectrum of the generated idlers together with an OSA trace of the 980 nm-band pump+signal. The position of the 1550 nm pump, which has been notch filtered, is denoted by a dashed line. c) Contour plot of the generated 1550 nm idler spectra (in units of detuning from the 1550 nm pump) for differing levels of 980 nm band pump-input signal detuning (taken with 0.2 nm tuning steps). d) Normalized idler power as a function of its wavelength for fixed pumps and tunable 980 nm input signal. The gray central region denotes the bandwidth of the 1550 nm pump rejection notch filter. e) Conversion efficiency (bottom) and converted idler and background count rate (top) as a function of the 1550 nm pump power inside the waveguide at its input. The error bars (often smaller than the data point size) are due to the variation in the detected SPAD count rates, and are one standard deviation values. The signal-to-background level for the converted idler increases from  $5.6 \pm 2.5$  at the lowest pump power to  $9.6 \pm 2.4$  at the highest pump power.

smaller detuning levels, high signal-to-background levels are generally harder to achieve. This can be due to technical reasons, such as incomplete suppression of the pump at the converted idler wavelength, or more fundamental reasons related to the waveguide system itself, such as spontaneous Raman scattering in  $\text{SiO}_2$  [22] or modulation instability when the strong pumps are situated in regions of anomalous dispersion. Assuming these effects contribute to the measured noise level, the relatively high signal-to-background levels observed suggest that the  $\text{Si}_3\text{N}_4$



system is less susceptible to noise from Raman scattering than systems such as silica optical fibers. If these signal-to-background levels can be maintained at higher conversion efficiency levels, they would be adequate for initial quantum frequency conversion experiments with true single photon sources (signal-to-background ratios between 2 and 7 were used in Ref. [10]).

In moving to such experiments, of principal concern is the very low conversion efficiencies thus far demonstrated. However, this experiment was done under continuous-wave and relatively low pump power conditions, with maximum powers of  $P_1 = 13$  mW and  $P_2 = 43$  mW at the input inside the waveguide. These results are similar to those in Ref. [16] achieved under similar power conditions. In that work, by using amplified pulses, the conversion efficiency improved to  $\approx 5$  % for peak powers of a few Watts coupled into the chip. With similar pump amplification (for example, using nanosecond pulses and an EDFA to generate the telecom-band high peak-power pump and a tapered amplifier for the 980 nm band pump), and by reducing the input coupling losses via optimized geometries (for example, inverse tapers in symmetrically clad coupling regions) - already demonstrated for  $\text{Si}_3\text{N}_4$  waveguides [23] - we expect the conversion efficiency to improve to over 25 %, as confirmed by split-step Fourier method simulations [16]. This conversion efficiency level would render the interface suitable for quantum frequency conversion with single photon emitters [10, 15].

#### 4. Experimental results - Wideband Frequency Upconversion

The flexibility of the two pump FWM-BS process implies that by switching the roles of the signal and idler, we can perform frequency upconversion within the same device. To ensure the capability of single photon counting in the 980 nm band, the 974 nm pump laser is heavily filtered via volume Bragg gratings to yield better than 140 dB of suppression. The 1550 nm fixed pump laser is combined with a tunable telecommunications-band weak signal via a 90:10 coupler, and the combined pumps+signal are multiplexed via a WDM and sent to the waveguide chip (Fig. 3(a)). The output of the chip is notch-filtered (to get rid of the strong 974 nm laser) and sent to either a visible-wavelength spectrometer or silicon SPAD for signal-to-background measurements.

Figure 3(b) shows the generated 980 nm band idlers for a specific set of pump and input signal wavelengths in the 1550 nm band (the 980 nm band pump has been removed by a notch filter after the chip, as shown in Fig. 3(b)). Combining a series of upconversion spectra as the 1550 nm band input signal is swept yields the contour plot shown in Fig. 3(c), which confirms a tuning of the generated idlers that matches the energy conservation condition,  $\omega_i = \omega_s \pm (\omega_1 - \omega_2)$ . By integrating the power within each idler peak, we can deduce the normalized conversion efficiency and hence the phase-matching bandwidth, which, as expected, is similar in behavior to that observed in downconversion (Fig. 2(d)). As the 1550 nm pump power is increased up to 50 mW, the internal conversion efficiency improves from -77 dB to -62 dB, while the signal-to-background ratio for the  $\omega_i^+$  idler reaches a maximum of  $\approx 20$  (Fig. 3(e)). As in the case of downconversion, the signal-to-background ratio is determined by measuring the counts in the  $\omega_i^+$  band with the input 980 nm signal turned on and off, and dividing the two values (after subtraction of the detector dark count rate of  $\approx 170$  s $^{-1}$ ). The higher signal-to-background we measure here for upconversion can most likely be attributed to the improved filtering of the pumps both at the input and the output of the waveguide via volume Bragg gratings that provide better extinction than fiber-based WDMs. This also provides some indication that the process may not be limited by noise contributions due to Raman scattering. In comparison to  $\text{SiO}_2$ , we note that Raman scattering in silicon nitride has not been observed to be comparable to four-wave-mixing, even at high power conditions [19, 23–25]. Another potential reason for the higher signal-to-background levels is that the strong 980 nm pump is situated deep within the normal dispersion region (Fig. 1(b)), so that modulation insta-

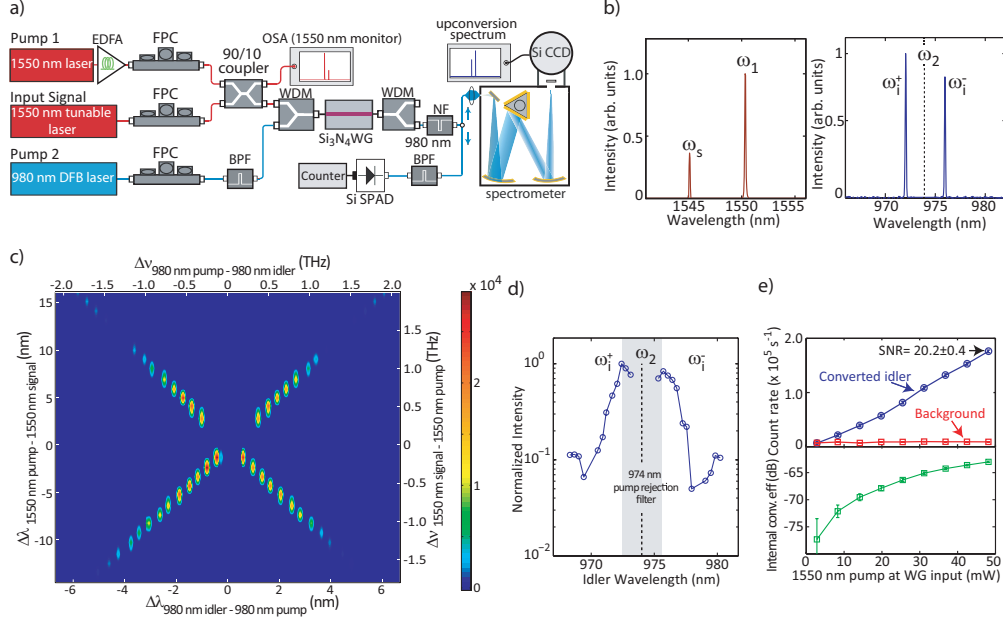


Fig. 3. a) Experimental setup for frequency upconversion from 1550 nm to 980 nm: A tunable 1550 nm signal laser is combined on a 90:10 coupler with a 1550 nm pump and then multiplexed (through a fiber 980 nm/1550 nm WDM) with a 974 nm pump laser. The output of the WDM is sent to the waveguide chip, and the output of the waveguide is notch-filtered to remove the residual 974 nm pump. The 1550 nm wavelengths are monitored on the OSA, while the converted 980 nm band idlers are measured on a spectrometer equipped with a Si CCD, or are bandpass filtered and measured on a Si SPAD. b) Sample spectrum of the generated idlers together with an OSA trace of the 1550 nm-band pump+signal. The position of the 974 nm pump, which has been notch filtered, is denoted by a dashed line. c) Contour plot of the generated 980 nm idler spectra (in units of detuning from the 974 nm pump) for different levels of 1550 nm band pump-input signal detuning (taken with 1 nm tunings steps). d) Normalized idler power as a function of its wavelength for fixed pumps and tunable 1550 nm input signal. The gray central region denotes the bandwidth of the 974 nm pump rejection notch filter. e) Conversion efficiency (bottom) and converted idler and background count rate (top) as a function of the 1550 nm pump power inside the waveguide and at its input. The error bars (often smaller than the data point size) are due to the variation in the detected SPAD count rates, and are one standard deviation values. The signal-to-background level for the converted idler increases up to  $20.2 \pm 0.4$  at the highest pump power.

bility is completely suppressed. In comparison, the 1550 nm pump, though nominally also in a region of normal dispersion, is much closer to the dispersion zero. As a result, deviations in the waveguide geometry with respect to the simulated structure (e.g., due to fabrication tolerances or a non-uniform waveguide cross-section along its length) may lead to modulation instability induced noise.

## 5. Experimental results - Narrowband Frequency Conversion

As noted previously, FWM-BS in the case of pumps that are far-detuned from the input signal and generated idlers has likely advantages from a signal-to-background perspective. To some



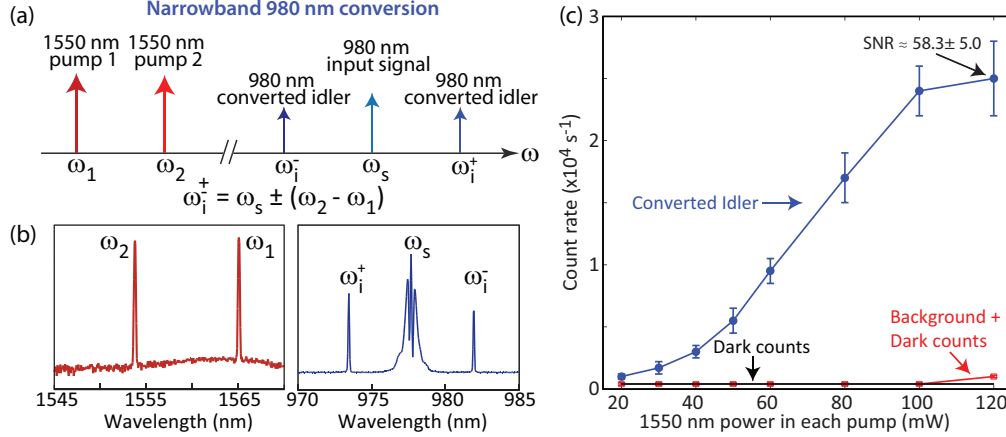


Fig. 4. a) FWM-BS process for nearly noise-free, narrowband frequency conversion: two telecommunications-band pumps cause a wavelength-exchange between a signal and its idler according to the energy conservation rule:  $\omega_i = \omega_s \pm (\omega_2 - \omega_1)$ . b) OSA spectrum of the telecommunications-band pumps and spectrometer record of the generated 980 nm band idlers (residual unconverted signal attenuated via fiber Bragg gratings). c) Converted idler and the corresponding background vs. waveguide input pump power. For the majority of the input power range, no excess noise above the SPAD dark count rate is observed. At the highest pump power, the signal-to-background ratio is  $\approx 50$ , and is limited by excess noise from the pump EDFA. The error bars are due to the variation in the detected SPAD count rates, and are one standard deviation values.

extent, it can thus provide a reference point for the best achievable signal-to-background levels within the system. To verify this, we revert to the narrowband conversion configuration (Fig. 4) we studied recently in Ref. [16]. Here, two telecommunications-wavelengths pumps  $\omega_1$  and  $\omega_2$  convert a 980 nm band input signal  $\omega_s$  to an idler  $\omega_i$  in the same band, according to the rule  $\omega_i = \omega_s \pm (\omega_2 - \omega_1)$ . At optimal conversion conditions, the pumps are separated by  $\approx 10$  nm, while the signal/idler are separated by  $\approx 5$  nm (Fig. 4(b)). We bandpass filter the generated idler  $\omega_i^+$  and use a Si SPAD to measure the power in this wavelength band with the input signal turned on and off (Fig. 4(c)). When the input is turned off, we measure no excess background counts above the SPAD dark count rate ( $\approx 400 \text{ s}^{-1}$ ) for the majority of the 1550 nm pump power range sent into the waveguide (so that after SPAD dark count subtraction, the process is noise-free). Even at the very highest pump powers, for which we observe significant excess noise in our EDFA, we measure signal-to-background levels of  $\approx 50$ .

## 6. Discussion

We have demonstrated the first steps towards a quantum interface for ultra-wide band frequency conversion, and shown how it is experimentally possible to translate photons from 980 nm to 1550 nm and back via FWM-BS in a CMOS-compatible platform. The goal of this work is to pave the way towards both high-efficiency devices that render on-chip frequency conversion of single photon emitters practical, as well as to provide design guidelines for down(up)conversion of photons from various quantum emitters via FWM-BS. While our devices targeted the 980 nm band which is the wavelength range of InAs quantum dot SPSs that we have employed in recent experiments [12,26], the ability to engineer the dispersion, coupled with the transparency of silicon nitride, allows for devices that in principle can target most common single photon

emitters.

Figure 5(a) is a table of common SPS emission wavelengths, with the required geometry of the waveguide to achieve phase matching for downconversion towards the 1550 nm telecommunications band. Along with linear phase-matching, of key importance is for the strong pump fields to be in regions of normal dispersion, to avoid the onset of modulation instability. This has been achieved here by simply tuning the waveguide width, while keeping the thickness fixed at 550 nm. Figure 5(b) shows the resulting dispersion parameter  $D = \frac{-2\pi c}{\lambda^2} \frac{d^2\beta}{d\omega^2}$  for the different optimized geometries, where the zero dispersion point, to a first approximation, is close to the average of the two pumps' wavelengths [17]. Finally, Fig. 5(c) shows an example of the results from a split-step Fourier simulation [27] in which we take into account the calculated dispersion to assess the efficiency of the frequency conversion process without the approximations that go into the analytic coupled-mode theory model (e.g., no pump depletion, no pump mixing, and no degenerate four-wave-mixing). The figure plots the conversion efficiency as a function of pump power (assumed to be equal for the two pumps) in the case of downconversion from 780 nm to 1550 nm. We see that a conversion efficiency of  $\approx 25\%$  can be achieved for approximately 9 W of power in each pump. Simulations reveal that conversion efficiencies  $\gtrsim 25\%$  can be achieved for the other sets of wavelengths considered, and the corresponding pump powers are listed in the table in Fig. 5(a). It should be noted that while 9 W is a relatively high power when considering continuous-wave sources, it is readily achievable by amplifying nanosecond pulses in saturated erbium-doped or semiconductor tapered amplifiers, making our chip-scale interface a practical prospect for conversion of single photon states of light from quantum emitters (particularly systems like semiconductor quantum dots, which have characteristic timescales on the order of 1 ns). Moreover, by implementing the structure in  $\text{Si}_3\text{N}_4$ , peak power is not limited by phenomena such as two-photon absorption, and hence such powers can be coupled to a  $\text{Si}_3\text{N}_4$  waveguide without major problems, as observed in experiment for few Watt level pumps in Ref. [16]. On the other hand, implementation of the four-wave-mixing Bragg scattering process in crystalline silicon waveguides could be of interest, in part due to its higher nonlinear refractive index than  $\text{Si}_3\text{N}_4$  [28, 29]. Such work would be limited to wavelengths  $> 1000$  nm

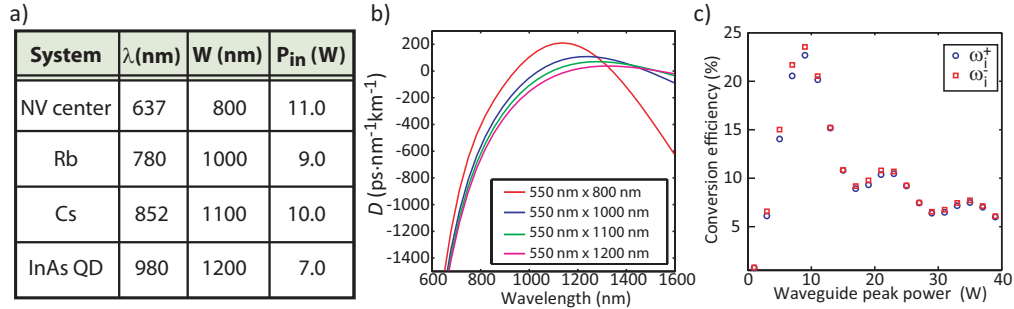


Fig. 5. a) Design parameters for  $\text{Si}_3\text{N}_4$ -on- $\text{SiO}_2$  waveguides targeting up(down)conversion between the telecommunications band and various single photon sources (SPSs) (Nitrogen vacancy center in diamond, Rubidium, Cesium, and InAs QD in descending order). The table specifies, for each SPS wavelength ( $\lambda$ ), the waveguide width (W) and the necessary input peak power ( $P_{in}$ ) for maximum conversion. The waveguide thickness has been fixed at 550 nm in all cases. b) The corresponding dispersion parameter  $D$  for each waveguide geometry. (c) Split-step Fourier simulation for the case of downconversion between 780 nm and 1550 nm. Conversion efficiency is plotted as a function of pump power, where the power in both pumps are assumed to be equal.

(as silicon is opaque at shorter wavelengths), and may require long wavelength ( $> 2000$  nm) pumps to avoid significant nonlinear absorption [30,31]. Alternately, materials like amorphous silicon, which combine high optical nonlinearity and a broader optical transparency window than silicon (though less than  $\text{Si}_3\text{N}_4$ ) may ultimately prove to be an attractive candidate for four-wave-mixing Bragg scattering within certain wavelength regions [32].

In conclusion, we have demonstrated a CMOS-compatible chip-scale interface for ultra-wide band frequency conversion via four-wave-mixing Bragg scattering in a silicon nitride waveguide, and characterized both its tuning bandwidth and noise properties. We performed proof-of-principle experiments demonstrating both downconversion and upconversion between the 980 nm and 1550 nm bands, rendering our chip a promising interface for connecting self-assembled InAs quantum dots to the telecommunications band. With improved input coupling and higher input pump peak powers, we expect our interface to be ready for frequency conversion of true single photon sources, which will be the target of future work.

## **7. Acknowledgments**

The authors thank Yoshitomo Okawachi for helpful comments on this work. I.A and S.A. acknowledge support under the Cooperative Research Agreement between the University of Maryland and NIST-CNST, Award 70NANB10H193. The authors also acknowledge the DARPA MESO program for partial support.